

Bunch-length Compressors

S. Di Mitri

Elettra – Sincrotrone Trieste, Trieste, Italy

Abstract

An introduction to radio-frequency and magnetic bunch length compression of ultra-relativistic particle beams in linear accelerators is given, with a treatment of the single-particle motion up to the second order, and attention to the production of high peak current bunches for free-electron lasers.

Keywords

Electron bunches; radio-frequency linear accelerators; electron optics.

1 Introduction

There is a growing demand for generating and transporting very short, high charge density electron bunches. Applications range from light sources driven by radio-frequency linear accelerators (RF linacs) such as free-electron lasers (FELs), to future linear colliders and novel electron-beam-driven acceleration schemes, e.g., dielectric- and plasma-wake-field-driven accelerators. The generation of hundreds of amperes peak current electron bunches directly out of an electron source is in conflict with the production of small transverse emittance beams, due to the repulsive interparticle Coulomb interactions ('space-charge' forces) that are especially effective at low beam energies. It is therefore preferable to create only a few tens of amperes peak current bunches at the source, such as an RF photo-injector, in order to dilute the charge density, and thereby ensure small transverse emittances. Beam manipulations are implemented then in the downstream transport line, at higher beam energies, in order to obtain short electron bunches while preserving the transverse emittance at the injector level. The process of manipulating an electron beam so to enhance its peak current is called, in short, bunch compression.

In this chapter, we introduce the reader to bunch-length compression by means of RF and magnetic insertions, with an analytical treatment of the single-particle motion up to second order in the particle coordinates. We pay special attention to the production of high peak current bunches for high-gain FELs. Other schemes aimed to produce short bunches have been proposed, either with a special design of the electron source or by selecting only one part of the bunch, e.g., via energy-dispersive collimation or spoiling. These latter techniques, however, are not addressed in this chapter.

2 Why FELs require high peak current bunches

Over the last decade several linac-driven FELs in the ultra-violet (UV) and X-ray wavelength ranges have been built, have met their design specifications and are now operating reliably in several laboratories around the world [1, 2]. One of the main factors contributing to this successful development has been the ability to create, accelerate, transport and control electron bunches of very high brightness.

The six-dimensional (6D) energy-normalized electron-beam brightness is defined as the total bunch charge divided by the product of the root-mean-square (rms) horizontal, vertical and longitudinal normalized emittances, barring numerical factors that can be found in the literature. Essentially, it is the beam charge density in the 6D phase space. For simplicity, particle motion is intended to be uncoupled, and each transverse emittance is meant to be 'projected', i.e., it is computed over the particles' coordinates projected onto the longitudinal z -coordinate internal to the bunch [3]. The normalized

transverse emittances scale as the product of beam size and angular divergence. The normalized longitudinal emittance scales as the product of bunch length and energy spread, the latter being in fact the particles' spread in longitudinal momentum. The transverse normalized emittances are invariant under acceleration and linear transport, presuming that collective effects, such as space-charge forces, can be neglected. The same is true for the longitudinal normalized emittance if the energy spread is purely uncorrelated (i.e., not correlated with z) and particles are in the ultra-relativistic approximation: in this case, neither the bunch length, σ_z , nor the beam energy spread, σ_E , vary during acceleration.

The presence of non-linear motion and collective effects along the beam-delivery system may dilute the rms normalized emittances from their values at the injection point [2]. By introducing an effective degradation factor $\zeta \geq 1$ in each plane of particle motion so that $\varepsilon_{nx,f} = \zeta_x \gamma_0 \varepsilon_{x,0}$, $\varepsilon_{ny,f} = \zeta_y \gamma_0 \varepsilon_{y,0}$ and $\varepsilon_{nz,f} = \sigma_{z,f} \sigma_{E,f} = \zeta_z \sigma_{z,0} \sigma_{E,0}$, we are able to relate the 6D normalized brightness at the undulator, $B_{n,f}$, to the one at the linac injection, $B_{n,0}$:

$$B_{n,f} = \frac{Q}{\varepsilon_{nx,f} \varepsilon_{ny,f} \varepsilon_{nz,f}} = \frac{Q}{\zeta_x \zeta_y \zeta_z \gamma_0^2 \varepsilon_{x,0} \varepsilon_{y,0} \sigma_{z,0} \sigma_{E,0}} = \frac{B_{n,0}}{\zeta_x \zeta_y \zeta_z}. \quad (1)$$

In the ideal case of vanishing non-linear and collective effects, $\zeta_x, \zeta_y, \zeta_z \rightarrow 1$, and the 6D normalized brightness is *preserved* at the injector level under acceleration and bunch-length compression.

The importance of electron-beam brightness for linac-driven high-gain FELs is underlined by the characteristic FEL parameter ρ , through which most of the one-dimensional (1D) FEL dynamics can be depicted [4]. In the so-called 1D, 'cold-beam' limit, where the effects on the FEL output of electron-beam energy spread, transverse emittance and radiation diffraction are all neglected, the radiation peak power at the resonant wavelength grows exponentially along the undulator with a gain length $L_G = \lambda_u / (4\pi\sqrt{3}\rho)$, where

$$\rho = \left(\frac{\Omega_p \lambda_u a_w [JJ]}{8\pi c \gamma} \right)^{2/3} = \frac{1}{2\gamma} \left(\frac{I}{I_A} \right)^{1/3} \left(\frac{\lambda_u a_w [JJ]}{2\pi \sigma_x} \right)^{2/3}, \quad (2)$$

Ω_p being the plasma frequency, γ the relativistic Lorentz factor for the electron-beam mean energy, λ_u the undulator period length, I the electron-bunch peak current, $I_A = 17045$ A the Alfvén current, σ_x the standard deviation of the (assumed round) electron-beam transverse size; $[JJ]$ is the undulator-radiation coupling factor [5], equal to 1 for a helically polarized undulator and to $[J_0(\xi) - J_1(\xi)]$ for a plane-polarized undulator, where J_0 and J_1 are Bessel functions of the first kind with argument $\xi = K^2 / (4 + 2K^2)$. Here a_w and K are defined in the expression for the FEL fundamental wavelength of emission [6]:

$$\lambda = \frac{\lambda_u}{2\gamma^2} (1 + a_w^2), \quad (3)$$

with $a_w = K$ for helically and $a_w = K/\sqrt{2}$ for plane-polarized undulators, and $K = eB_0 \lambda_u / (2\pi m_e c) = 0.934 B_0 [\text{T}] \lambda_u [\text{cm}]$, in practical units, is the so-called undulator parameter, B_0 the undulator peak magnetic field, e and m_e the electron charge and rest mass, respectively, and c the speed of light in vacuum. K is linearly proportional to the electron's amplitude of transverse oscillation in the undulator field and is typically in the range 1–5. Equation (3) is often referred to as the FEL 'resonance condition' since it selects, for any undulator period and magnetic field strength, the necessary electron beam energy for lasing at λ .

For kA-current beams, typically $\rho \approx 10^{-3}$ in the UV range, and it drops to $\sim 10^{-4}$ in the X-ray range. If the undulator length $N_u \lambda_u$, with N_u the number of undulator periods, is equal to or longer than $\sim 20L_G$, the conversion of electrons' kinetic energy to photon energy considerably enlarges the electron-beam energy spread, with an eventual reduction in the FEL gain [6]. When the FEL process starts up from noise in the electron-charge distribution – it is therefore said to operate in self-amplified spontaneous emission (SASE) mode [7, 8] – the associated FEL power saturates at a level $P_{\text{sat}} \approx 1.6\rho EI/e$. In spite of the low FEL extraction efficiency relative to the electron-beam power (because $\rho \ll 1$), an electron beam at multi-GeV energies and kA-scale peak currents is able to produce multi-GW-scale radiation peak power. For SASE devices, the value of ρ also defines the approximate number of undulator periods $N_{\text{sat}} \approx 1/\rho$ and the length $L_{\text{sat}} \approx \lambda_u/\rho$ necessary to reach power saturation. The normalized spectral bandwidth at saturation is $\Delta\omega/\omega \approx \rho$, presuming a more or less mono-energetic electron beam with little z -correlated energy spread.

Equation (2) suggests that a smaller beam transverse emittance, which is proportional to the square of the beam transverse size, is associated with a higher FEL gain. In fact, the most efficient electron–photon beam interaction occurs when the transverse beam phase space area and distribution match those of the emitted radiation. This is also the condition for maximum transverse coherence of FEL radiation, and it translates into an electron-beam emittance at the undulator smaller than or of the same order as the one of the diffraction-limited photon beam [9]:

$$\varepsilon_{x,y} \leq \frac{\lambda}{4\pi} . \quad (4)$$

By substituting Eqs. (3) and (4) (with the beam emittance at the diffraction limit) into Eq. (1), we can establish a relationship between $B_{n,f}$ and λ [10]:

$$B_{n,f} = \frac{Q}{\varepsilon_{nx,f} \varepsilon_{ny,f} \varepsilon_{nz,f}} = \frac{I}{c\sigma_E \gamma_0^2 \varepsilon_0^2} \approx \frac{I}{\lambda \sigma_E} \frac{32\pi^2}{c\lambda_u (1+a_w^2)} . \quad (5)$$

It is worth noticing that the ratio I/σ_E is invariant under acceleration and compression, when collective effects are ignored. So, for any given undulator, efficient lasing at shorter λ requires a higher $B_{n,f}$. This is confirmed by Fig. 1, where $B_{n,f}$ of designed and existing single-pass linac-driven FEL facilities is shown as a function of the maximum photon energy (i.e., minimum fundamental wavelength) from UV to X-rays.

At this point one might wonder why a high peak current is required at the undulator, if the FEL dynamics appears to be so tightly related to the 6D normalized electron-beam brightness, the latter one being approximately invariant for a well-set beam-delivery system. The fact is that, as long as the beam effective rms *relative* energy spread is smaller than ρ (here ‘effective’ refers to the contribution of both beam transverse emittance and spread in longitudinal momentum to the lack of synchronism between the electrons and the radiation emitted in the undulator [6]), the FEL dynamics is well depicted by the 1D cold-beam model in Eq. (2). We therefore see that the higher the peak current, the larger the FEL gain, the shorter the saturation length. The relatively weak dependence of ρ on I is one of the reasons why ρ typically spans over one order of magnitude only, for lasing from UV to hard X-rays, whereas I has typically to be increased from a few tens of amperes out of photo-injectors to kA level at the undulator. With the common prescription of *relative* energy spread $\sigma_\delta < 0.5\rho$ in mind for maximum FEL gain [6], it makes sense to collapse the electron-beam quality into the 5D normalized brightness, which is just $B_{n,f} \times \sigma_E$. This quantity is *not* invariant under compression, and is actually linearly proportional to the bunch length total compression factor.

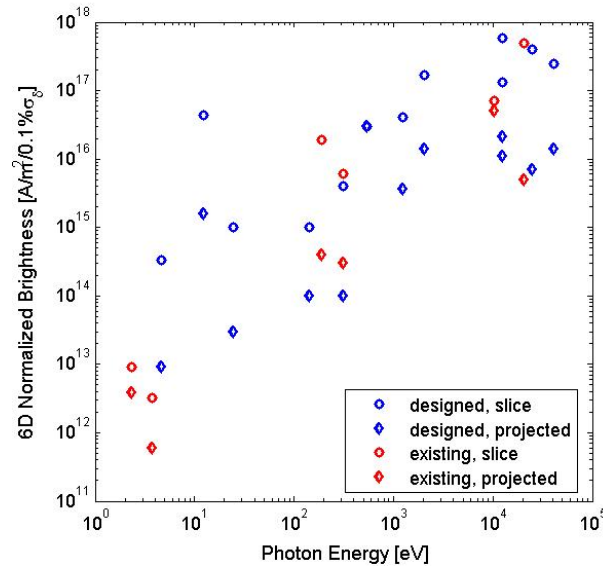


Fig. 1: 6D normalized electron-beam brightness (Eq. (1)) vs. maximum photon energy at fundamental FEL emission, for facilities in the UV to X-rays, in design stage (blue) or operational (red), up to 2013. From lower to higher photon energies, “existing” facilities are: SPARC (Italy), SDUV-FEL (China), FLASH-I (Germany), FERMI (Italy), LCLS (USA), SACLA (Japan). The brightness refers to the projected (circle) or slice value in the bunch (diamond). Published in Ref. [2]. Copyright of Elsevier.

In summary, bunch-length compression is required for increasing the bunch peak current from the injection level by usually one to three orders of magnitude, and eventually driving a *high-gain* FEL, given that transverse emittances and relative energy spread are kept small at the undulator. In the following we will focus on RF and magnetic bunch-length compression of ultra-relativistic electrons. As we will see, RF compression is achieved by exploiting the longitudinal slippage of electrons in an RF linac, at beam energies typically lower than ~ 100 MeV. A magnetic compressor is made of an RF linac followed by a magnetic insertion including dipole magnets, and the electrons’ longitudinal slippage happens in the magnetic insertion only. Magnetic compression is commonly achieved at beam energies higher than ~ 100 MeV. An exhaustive literature on bunch-length compression is available, and some fundamental references are provided in this chapter. Still, we will introduce the reader to the salient topics related to the single-particle dynamics, and will illustrate the basic equations of motion.

3 Particle motion in a RF linac

We consider the motion of ultra-relativistic particles in an RF linac made, for example, of copper structures with inner iris. We assume each structure made of identical cylindrical cells; the RF power flows through the cells, and is eventually extracted on a load. Such structures behave like waveguides of cylindrical symmetry, and the longitudinal electric field component, which has in general a radial dependence, is a superposition of n field harmonics characterized by an angular RF frequency ω and by an RF wave-number k [11]:

$$\begin{aligned} E_z^{\text{TW}} &= \sum_{n=-\infty}^{+\infty} a_n J_n(k_{r,n} r) \cos(\omega t(z) - k_n s + \varphi) \cong E_{z,0}^{\text{TW}} \cos(\omega t_{\text{syn}} + \omega \Delta t - ks + \varphi) \\ &= E_{z,0}^{\text{TW}} \cos(\omega t_{\text{syn}} - ks + \varphi + kz) \equiv E_{z,0}^{\text{TW}} \cos(\phi_{\text{rf}} + kz), \end{aligned} \quad (6)$$

where the generic particle time coordinate $t(z)$ was expanded in the arrival time t_{syn} of the reference (or synchronous) particle, e.g. the bunch centroid, plus the arrival time of the generic particle with respect to it. We then used the identity $\omega \Delta t = kz$. The z -coordinate runs inside the bunch, with $z = 0$ for the

reference particle. The s -coordinate runs along the electric axis of the cell. The arbitrary phase φ determines the arrival time of the reference particle relative to the electric field inside the cell. Finally, we defined the RF phase $\phi_{\text{rf}} = \omega t_{\text{syn}} - ks + \varphi$, which tends to be constant for ultra-relativistic beams.

The last term of Eq. (6) describes the fundamental on-axis mode of the longitudinal electric field in a ‘travelling wave’ (TW) accelerating structure. In fact, we assume that the transverse beam sizes are much smaller than the structure inner radius, and that the beam is well centred on the structure’s electric axis. Moreover, most of the acceleration is provided by the fundamental mode of the field.

If the structure is made in order to allow reflections of the RF power, we calculate the resulting net positive interference of two counter-propagating waves as follows:

$$\begin{aligned} E_z^{\text{SW}} &\cong E_{z,0}^{\text{TW}} \cos(\omega t(z) - ks + \varphi) + E_{z,0}^{\text{TW}} \cos(\omega t(z) + ks + \varphi) \\ &= 2E_{z,0}^{\text{TW}} \cos(\omega t_{\text{syn}} + \omega \Delta t + \varphi) \cos(-ks) \\ &\equiv E_{z,0} \cos(\omega t_{\text{syn}} + kz + \varphi) \cos(ks) . \end{aligned} \quad (7)$$

Equation (7) describes the on-axis longitudinal electric field in a ‘standing wave’ (SW) structure. We now assume that the electric field is approximately uniform across the cell gap (i.e., $\cos(ks) \approx \text{const.}$), and that the reference particle’s velocity v , as well as those of all other particles, does not change substantially during acceleration (ultra-relativistic limit). Then the generic particle energy gain through a cell of coordinates $[-g/2, g/2]$ is

$$\begin{aligned} \Delta E(g, z) &= -e \int_{-g/2}^{g/2} E_z^{\text{SW}} ds = -e E_{z,0} \int_{-g/2}^{g/2} ds \left[\cos(\omega t_{\text{syn}}) \cos(kz + \varphi) - \sin(\omega t_{\text{syn}}) \sin(kz + \varphi) \right] \\ &= -e E_{z,0} \int_{-g/2}^{g/2} ds \left[\cos(\omega s/v) \cos(kz + \varphi) - \sin(\omega s/v) \sin(kz + \varphi) \right] \\ &= -e E_{z,0} g \frac{\sin\left(\frac{\omega g}{2v}\right)}{\left(\frac{\omega g}{2v}\right)} \cos(kz + \phi_{\text{rf}}) \equiv e \Delta V_0(g) T \cos(\phi_{\text{rf}} + kz) . \end{aligned} \quad (8)$$

T is called the ‘transit-time factor’; it is always less than 1 (typically in the range 0.85–0.95) and it describes the reduction of energy gain because of the time variation of the electric field along the cell, when the beam traverses the cell with a finite velocity $v < c$. In the following, for the sake of brevity, we will collapse T into an effective electric potential ΔV_0 . It is worth noticing that the final expression for the energy gain in Eq. (8) applies to a TW as well with $T = 1$, where the TW structure is assumed to be tuned in order to maintain the synchronism between the RF field and the reference particle.

Finally, we notice that the first equality in Eq. (7) can be rewritten as $E_z^{\text{SW}}(z = 0) \cong E_{z,0}^{\text{TW}} [\cos(\phi_{\text{rf}}) + \cos(\phi_{\text{rf}} + 2ks)]$. This tells us that a particle travelling in synchronism with the forward wave at the light speed experiences both a constant accelerating force and an oscillating force from the backward wave. The latter has a double oscillation frequency, and it does not contribute to beam motion on average. Henceforth, we keep the notation according to which beam acceleration (i.e., acceleration sampled by the reference particle) is maximum for $\phi_{\text{rf}} = 0$: in this case the beam is said to be ‘on-crest’ of the RF wave. As we will see in the next section, magnetic bunch-length compression requires a correlation of the particles’ energy with their longitudinal positions inside the

bunch (see Figs. 3 and 4 below), and such a correlation is established by operating the linac ‘off-crest’, namely at an RF phase $-\pi < \phi_{\text{rf}} < 0$ or $0 < \phi_{\text{rf}} < \pi$, depending on the geometry of the downstream magnetic insertion. The special point $\phi_{\text{rf}} = \pm \pi/2$ is commonly called ‘zero crossing’. Accelerated either on-crest or off-crest, we assume that the beam longitudinal phase space (z, E) is mainly determined by the curvature imposed by the cosine-like behaviour of the accelerating field.

The coefficient used to quantify the linear correlation in (z, E) is named ‘linear energy chirp’, and it can be evaluated by expanding the electric field-induced energy gain in Eq. (8) to first order in z :

$$\begin{aligned} h &\equiv \frac{1}{E_0} \frac{dE}{dz} \cong \frac{1}{E_i + e\Delta V_0 \cos \phi_{\text{rf}}} \frac{d}{dz} \left[E_i + e\Delta V_0 \cos(\phi_{\text{rf}}) - e\Delta V_0 k z \sin(\phi_{\text{rf}}) + o(z^2) \right] \\ &= -\frac{e\Delta V_0 k \sin \phi_{\text{rf}}}{E_i + e\Delta V_0 \cos \phi_{\text{rf}}}, \end{aligned} \quad (9)$$

where the beam is injected into the linac with a mean energy E_i . When the beam energy spread induced by the RF curvature is much larger than the uncorrelated energy spread, which depends on the process of beam generation, we may estimate $|h| \approx \sigma_\delta / \sigma_z$. As a consequence, as long as the beam correlated energy spread is constant when the bunch length is shortened (or lengthened) in a magnetic insertion, the energy chirp is increased (or lowered) by the same compression factor.

4 Particle motion in a magnetic chicane

By evaluating the Lorentz force for a particle with longitudinal momentum p_z traversing a dipole magnet with uniform vertical field B_0 , one finds that the radius of curvature R of the particle’s trajectory depends on the magnetic field and the momentum according to $p_z [\text{GeV}/c] = 0.2998 B_0 [\text{T}] R[\text{m}]$. This suggests that particles with different momentum will follow different (longer vs. shorter) orbits. Since the longitudinal velocity of all particles is assumed to be very close to c independently from their spread in energy, the particles will arrive at a longitudinal position s downstream of the magnet at different times. In other words, the longitudinal coordinate z of particles inside the bunch is changed. We therefore envision a way to shorten or lengthen the bunch, with a suitable arrangement of energy spread and dipole magnets. The former is manipulated with an RF linac as depicted in the previous section. In particular, the energy spread is correlated along the bunch so that, for example, less energetic particles in the bunch head will follow orbits longer than more energetic particles in the bunch tail, as shown in Fig. 2. At the exit of the magnetic insertion, the bunch head and tail will have been caught towards the bunch centre, and the bunch length will be shortened. The final aim of bunch-length compression, as explained in Section 2, is that of increasing the bunch peak current.

In linacs driving single-pass FELs, it is usually convenient to maintain the beam trajectory on a straight path, which is also the electric axis of the accelerating structures. For this reason dipole magnets devoted to bunch compression are arranged in geometries that do not provide a net beam deflection, such as a four-dipole chicane. We first consider a symmetric geometry made of identical dipoles, as shown in Fig. 2. In each dipole of length l_d , the bending angle of the reference (on-momentum) particle is $|\theta_0| = l_d / R = eB_0 l_d / p_{z,0}$, and the total deflection angle through the chicane is $\theta_{0,1} + \theta_{0,2} + \theta_{0,3} + \theta_{0,4} = 0$. For a generic off-momentum particle the bending angle is $\theta = eB_0 l_d / (p_{z,0} + \Delta p_z) \equiv \theta_0 / (1 + \delta)$, and still the net deflection through the chicane is zero. The same result holds for an expansion of the total bending angle to any order in δ .

We now assume that when particles are travelling in the drift section upstream of the chicane, their transverse position and angular divergence do not depend on their energy difference, i.e. the energy-dispersion function and its first derivative w.r.t. s , evaluated at the entrance of the chicane, are both zero [12]: $\eta_x(s=0) = \Delta x/\delta \equiv 0, \eta'_x(s=0) = \Delta x'/\delta \equiv 0$. For symmetry, those functions are also zero at the chicane exit. Naively, this means that particles lying on a line at the entrance of the chicane and with no angular divergence still lie on a line at the chicane exit, regardless of their spread in energy (see Fig. 2). Such a property defines the chicane as an ‘achromatic’ line. Since the total bending angle of an off-momentum particle through the chicane is zero at all orders in δ , as demonstrated above, such a chicane is achromatic at all orders (barring magnets’ errors or geometry imperfections).

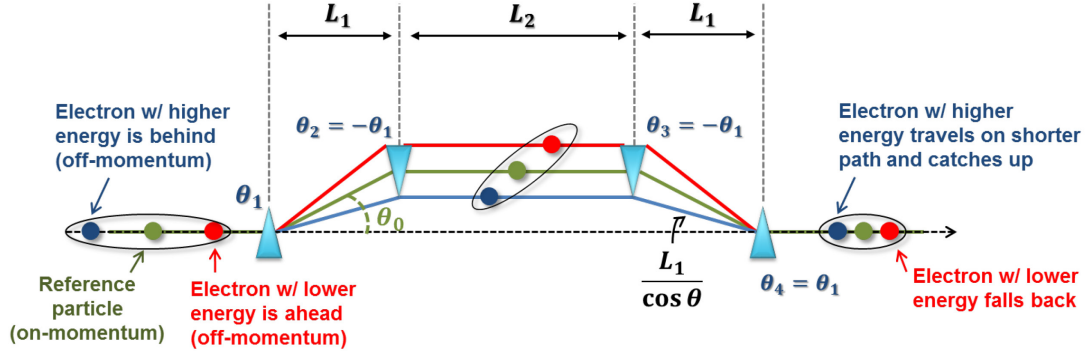


Fig. 2: Geometry (not to scale) of a four-dipole symmetric magnetic chicane, and particles’ motion through it for the case of bunch-length compression. See context for the meaning of symbols.

In accelerator physics, the evolution of particle 6D coordinates through an arbitrary beam line is commonly depicted through the matrix formalism [12], i.e., each element of the beam line is depicted through a matrix whose terms depend on the element’s parameters and geometry. A beam line made of consecutive elements is represented by a matrix that is the ordered product of the individual ones. Thus, the dependence of a particle’s z -coordinate at the exit of the chicane on its momentum deviation can be written as $z_f(\delta) = z_i + R_{56}\delta$, with R_{56} the chicane matrix element. We now calculate R_{56} looking at the particle longitudinal slippage $\Delta z = z_f - z_i$, through the chicane, for the geometry shown in Fig. 2, and assuming once more ultra-relativistic particles.

We neglect for the moment the length of dipole magnets with respect to other lengths of the chicane involved. The path length of an off-momentum particle through the chicane is $s_z = \frac{2L_1}{\cos \theta} + L_2$, and the one of the on-momentum particle $s_{z,0} = \frac{2L_1}{\cos \theta_0} + L_2$. Their path-length difference, i.e. the longitudinal slippage of the off-momentum particle w.r.t. the on-momentum one, at the exit of chicane, is

$$\begin{aligned} \Delta s &= s_z - s_{z,0} = 2L_1 \left(\frac{1}{\cos \theta} - \frac{1}{\cos \theta_0} \right) \cong L_1 (\theta^2 - \theta_0^2) + o(\theta^4) = -L_1 \theta_0^2 \left[1 - \frac{1}{(1+\delta)^2} \right] + o(\theta^4) \\ &\cong -2L_1 \theta_0^2 \delta + o(\theta^4, \delta^2). \end{aligned} \quad (10)$$

Equation (10) tells us that $R_{56} = \frac{\Delta z}{\delta} \cong -2L_1 \theta_0^2$ for $\theta_0 \ll 1$; namely, at first order in δ the bunch-length shortening is quadratic with the dipoles’ bending angle, and does not depend on the drift length in between the inner dipoles (in that region, particles are travelling on parallel trajectories at the same velocity, and therefore they do not slip one with respect to the others). When the path length in non-

zero-length dipoles is included, we find $R_{56} \cong -2\theta_0^2 \left(L_1 + \frac{2}{3}l_d \right)$. More accurate expressions can be found in the literature [13].

There is an intrinsic connection between R_{56} and the energy-dispersion function (henceforth, simply dispersion), which we explicit below. Let us introduce the ‘momentum compaction’ factor of a dispersive beam line, i.e., the particle’s relative variation of path length per relative momentum deviation, $\alpha_c \equiv \frac{\Delta L/L_0}{\delta}$. In a dipole magnet we have $\Delta L = (R_0 + \Delta x)\theta - R_0\theta_0 \cong \Delta x\theta_0$ for $\Delta\theta = (\theta_0 - \theta) \rightarrow 0$, with R_0 the curvature radius of the on-momentum particle, and Δx the lateral distance in the bending plane of the off-momentum particle from the reference trajectory. Hence, we obtain $\alpha_c \cong \frac{1}{R_0} \frac{\Delta x}{\delta}$. For R_{56} we find

$$R_{56} = \frac{\Delta z}{\delta} \cong \frac{\Delta L}{\delta} = \alpha_c L_0 \rightarrow R_{56}(s) = \int_0^s \alpha_c(s') ds' = \int_0^s \frac{1}{R(s')} \frac{\Delta x(s')}{\delta} ds' = \int_0^s \frac{\eta_x(s')}{R(s')} ds', \quad (11)$$

where we have retained a generic dependence of the bending radius on the s -coordinate, and we used the definition of dispersion function introduced above. Equation (11) holds for an arbitrary beam line, and it shows that longitudinal slippage of particles only happens in the presence of curvature, i.e., inside dipole magnets. At the same time, manipulation of the dispersion function in between consecutive dipoles (e.g., through a suitable distance between dipoles of a chicane, or with additional quadrupole magnets in between them) allows R_{56} of the system to be tuned.

We finally point out that if particles are not in the ultra-relativistic regime, i.e., their longitudinal velocity varies with their longitudinal momentum, then an effective particles’ slippage also happens in a drift section. It can be shown that the drift section is characterized by a matrix element:

$$R_{56} = \frac{\Delta z}{\delta} = -\Delta L \frac{p_{z,0}}{\Delta p_z} = -L_0 \frac{\Delta\beta_z}{\beta_{z,0}} \frac{\beta_{z,0}}{\gamma_0^2 \Delta\beta_z} = -\frac{L_0}{\gamma_0^2}, \quad (11a)$$

where the suffix ‘0’ refers to the reference particle. At low beam energies, this term may become important. If applied to a chicane, L_0 refers to the path length through the whole line.

5 Bunch-length linear compression factor

We now consider a particle motion in the chicane of Fig. 2. We differentiate the particle longitudinal slippage, evaluated through the whole chicane, and keep only terms to first order in the particle coordinates (linear approximation):

$$\begin{aligned} dz_f &= dz_i + R_{56} d\delta \cong dz_i + R_{56} \frac{dE}{E_0} = dz_i \left(1 + R_{56} \frac{1}{E_0} \frac{dE(z)}{dz_i} \right) + R_{56} \frac{dE_{\text{unc}}}{E_0} \\ &= dz_i (1 + h_1 R_{56}) + R_{56} \delta_{\text{unc}} \equiv dz_i / C + R_{56} \delta_{\text{unc}}. \end{aligned} \quad (12)$$

In Eq. (12), E_0 is the electron beam mean energy at the compressor and δ is the energy deviation relative to E_0 . We have split the particle energy deviation into two terms, one for the energy deviation correlated with z , which translates into the initial linear energy chirp h_1 , and the other one for the initial uncorrelated energy deviation, δ_{unc} . Equation (12) defines the *linear* compression factor $C = (1 + h_1 R_{56})^{-1}$. It is worth noticing that $C \rightarrow \infty$ for $R_{56} = -1/h_1$. However, even in that limit, the actual bunch length is finite and

reaches the minimum rms value $\sigma_{z,\min} = R_{56}\sigma_{\delta,\text{unc}}$ by virtue of a non-zero δ_{unc} . Thus, ‘full’ compression at higher beam energies would result in shorter minimum bunch lengths. With accepted convention, the chicane geometry in Fig. 2 provides $R_{56} < 0$, and therefore the bunch length is shortened if $h_i > 0$, namely if the bunch head has a lower energy than the bunch tail. If a non-linear energy chirp is present (E depends on z at higher orders in z), we expect $h_i(z)$ to vary along the bunch, and so will C .

The uncorrelated energy spread plays an important role in the build up of the FEL instability, and for this reason it is convenient to point out its evolution during the compression process. In practical situations the linearly correlated energy spread is controlled through a proper setting of the linac RF phase. Quadratic and cubic components may require more sophisticated beam manipulations – such as acceleration through higher harmonic RF frequency structures or shaping the bunch current profile – which are not considered at the moment.

We write down the total relative energy spread of a generic particle as the sum of an uncorrelated term (δ_u) and a z -correlated term (δ_c), the latter being the beam energy chirp times the particle z -position. The *total* energy spread is assumed constant through the chicane (only magnetic fields are involved, and no frictional forces), and the final bunch length is expressed as a function of the initial one through the definition of C given above:

$$\delta_{\text{tot}} = \delta_{u,i} + \delta_{c,i} = \delta_{u,i} + h_i \Delta z_i \equiv \delta_{u,f} + h_f \Delta z_f = \dots = \delta_{u,f} + Ch_i \left(\frac{\Delta z_i}{C} + R_{56} \delta_{u,i} \right) + o(\delta^2, \Delta z^2). \quad (13)$$

By equating the third and the last terms of Eq. (13), and then passing to the rms value of the quantities involved, we find $\sigma_{u,f}^2 = \sigma_{u,i}^2 (1 - Ch_i R_{56})^2 = C^2 \sigma_{u,i}^2$, i.e., the uncorrelated energy spread is increased by the same factor C by which the bunch length is shortened. This result is often referred to as ‘preservation of longitudinal emittance’ because, when the energy chirp is removed (virtually or in reality) from the phase space, the longitudinal emittance is just the product of bunch length and uncorrelated energy spread. The product is constant, in fact, in the approximation of linear motion and absence of frictional forces. An illustration of the preservation of the longitudinal emittance for ‘undercompressed’, ‘fully compressed’ and ‘overcompressed’ beams is given in Fig. 3.

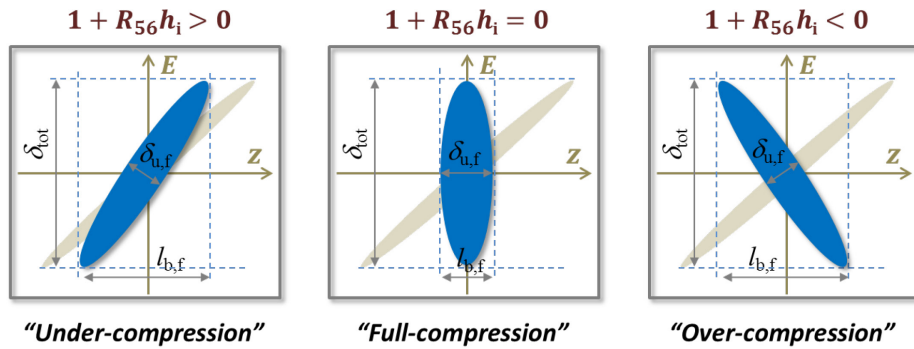


Fig. 3: Sketch of beam longitudinal phase space (ellipses) before (grey shadow) and after (blue) a magnetic chicane. Following accepted convention, $R_{56} < 0$ and bunch head is at $z < 0$; therefore, a positive chirp h_i at the entrance of the chicane (bunch head at lower energy) leads to bunch shortening. The ‘undercompression’ scenario on the left is the prevalent mode of operation of FEL linac drivers. When $h_i = -1/R_{56}$, the longitudinal phase space at the chicane exit is upright (plot at centre), and the bunch length l_b reaches its minimum value as set by the uncorrelated energy spread δ_u . If $h_i > 0$ but R_{56} is so negative that $1 + R_{56} h_i < 0$, then the bunch head and tail flip their longitudinal positions, and the energy chirp at the chicane exit has changed its sign. This is the case of ‘overcompression’ (right-hand plot), in which the bunch surpasses the point of ‘full compression’, and therefore the final bunch length is longer than its minimum value. In the absence of frictional forces (collective effects), the total energy spread δ_{tot} is constant through the chicane, as well as the beam longitudinal emittance, represented by the area of the ellipses.

6 Bunch-length compression at second order and linearization

Quadratic and even cubic components of the energy chirp, as anticipated above, may play an important role in the compression process, as C is no longer constant through the bunch, and different longitudinal portions of the bunch (slices) may be compressed in a different manner. Such a dynamics would imply that the current profile before compression (e.g., uniform, parabolic, Gaussian, etc.) is not preserved by the compression process. The situation is additionally deteriorated by a higher order dispersion function that translates into a higher order momentum compaction (T_{566} term at second order, U_{5666} at third order etc). In order to evaluate such a non-linear dynamics, we start expanding the expression for the energy gained by a generic particle in an RF linac to second order in z . For illustration, we ignore at this stage the second-order momentum compaction in the chicane. As already done for Eq. (8), we find

$$E_1 \cong E_i + e\Delta V_0 \cos \phi_{\text{rf}} - e\Delta V_0 k z \sin \phi_{\text{rf}} - \frac{e\Delta V_0}{2} k^2 z^2 \cos \phi_{\text{rf}} + o(z^3). \quad (14)$$

The second-order term in z of Eq. (14) can be cancelled by means of an additional RF component, but with different RF wavenumber:

$$\begin{aligned} E_2 &= E_1 + e\Delta V_{\text{H}} \cos(k_{\text{H}} z + \phi_{\text{H}}) \\ &\cong E_1 + e\Delta V_{\text{H}} \cos \phi_{\text{H}} - e\Delta V_{\text{H}} k_{\text{H}} z \sin \phi_{\text{H}} - \frac{e\Delta V_{\text{H}}}{2} k_{\text{H}}^2 z^2 \cos \phi_{\text{H}} + o(z^3). \end{aligned} \quad (15)$$

By comparing Eqs. (14) and (15), we find that the quadratic term generated by the additional structure(s) has to be positive, i.e., $\cos \phi_{\text{H}} < 0$ (say, $\phi_{\text{H}} = \pi$) and therefore the zeroth-order term from the additional linac is *decelerating* the beam. The new linac voltage has to satisfy $\Delta V_{\text{H}} = \frac{k^2}{k_{\text{H}}^2} \Delta V_0 \cos \phi_{\text{rf}}$.

Thus, compensation of the second-order energy chirp ('RF curvature') and net beam acceleration can only be achieved simultaneously if the RF wavenumber of the additional linac (often named 'linearizer') is larger than the one of the baseline accelerator. The scaling of the linearizer peak voltage with the wavenumber favours this approach, as long as the ratio of wavenumbers is 1/3 or smaller. For example, a baseline RF linac running in the S-band 3 GHz RF and providing 200 MeV energy gain, can be supplied by an additional X-band 12 GHz RF structure with peak voltage at ~15 MV level.

As anticipated above, we have so far ignored the non-linear z -motion of particles through the chicane, which is depicted by $z_{\text{r}}(\delta) = z_i + R_{56}\delta + T_{566}\delta^2$ up to second order. In a more complete analysis, the energy deviation in this expression combines with the expression for the energy chirp up to second order. In this more general and realistic case, linearization does not apply to the longitudinal phase space at the entrance of the chicane only, but to the compression process as a whole, through the RF linac *and* the chicane. As a result of cancellation of all second-order terms in the particles' dynamics, we expect that the current profile at the exit of the chicane resembles the one at its entrance, just squeezed in the z -coordinate. It can be shown [14] that cancellation of all the second-order terms for the special case $\cos \phi_{\text{H}} = -1$ implies $bR_{56} + a^2T_{566} = 0$, with $a = -\frac{e\Delta V_0}{E_i} \sin \phi_{\text{rf}}$ and $b = -\frac{e\Delta V_0 k^2 \cos \phi_{\text{rf}} + e\Delta V_{\text{H}} k_{\text{H}}^2}{2E_i}$.

By imposing that the beam mean energy at the chicane, E_{BC} , and the final bunch length do not change w.r.t. the case of purely linear motion, and additionally ignoring the contribution of the uncorrelated energy spread to the final bunch length, we find the necessary peak voltage of the harmonic cavity [14]:

$$e\Delta V_H = \frac{1}{\left(k_H^2/k^2 - 1\right)} \left\{ E_{BC} \left[1 + \frac{2}{k^2} \frac{T_{566}}{|R_{56}|^3} \left(1 - \frac{1}{C} \right)^3 \right] - E_i \right\}. \quad (16)$$

Figure 4 shows beam longitudinal phase-space and peak-current profiles simulated with the 1D tracking code LiTrack [15] up to second order, in the first stage of the FERMI FEL linac. The linac upstream the four-dipole chicane is set at 26 deg S-band far from the crest. With no X-band cavity, the RF curvature leads to a current spike in the bunch head, and to a ramped current profile at much lower level. A uniform current profile is recovered with an X-band cavity voltage of -15 MV.

Although Eq. (16) is valid for a one-stage compression only, the dependence of the linearizer peak voltage on the RF wavenumber is the same for multistage compression schemes. Moreover, when two chicanes or more are adopted, the peak-voltage setting of the linearizer does not vary much because after the first chicane, at lower energy, the bunch is shorter and less vulnerable to RF curvature [16]. A semi-analytical treatment of linearization of the compression process through RF cavities in the presence of higher order beam dynamics and single-bunch collective effects (e.g., short-range geometric wake fields [17]) can be found in Ref. [18].

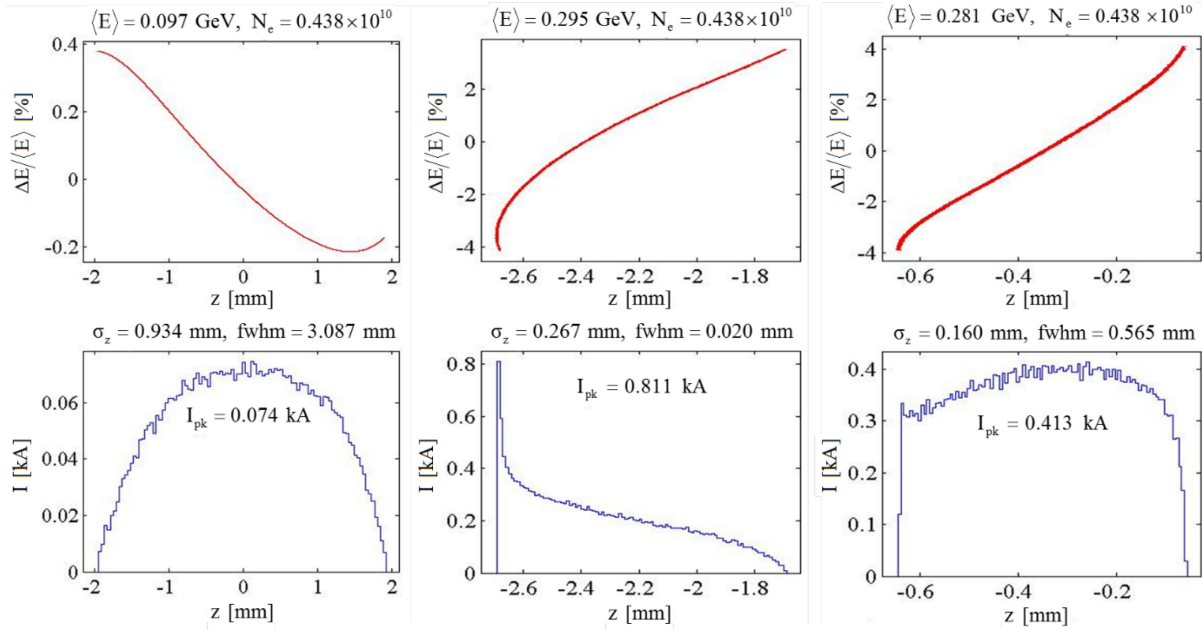


Fig. 4: Longitudinal phase space (top row) and current profile (bottom row) of a 700 pC charge bunch injected into the S-band FERMI FEL linac at 97 MeV (left). Centre plots are for the beam after magnetic compression in a four-dipole chicane, with no linearizer included. Right-hand plots are for the same beam when an X-band cavity in the upstream linac is set to -15 MV, for linearization of the compression process. Simulations were done with LiTrack code and up to second order.

Compensation of third-order terms is also possible by running the linearizer off-crest. However, the third-order energy chirp is commonly generated in the beam injector by space-charge forces (at energies typically lower than 5 MeV for photocathode RF injectors), and is of a sign [19] that is difficult to cancel without also partially cancelling the linear energy chirp necessary for compression, resulting in either inefficient acceleration or insufficient compression factor.

Alternative methods for the linearization of the compression process include passive dielectric-lined insertions or magnetic elements. In the former case, an optimum longitudinal voltage loss over the length of the bunch can be provided in order to compensate both the second-order RF time curvature and the second-order momentum compaction term [20]. Removal of second-order non-linearities in the

longitudinal phase space through optical elements is typically dealt with by sextupole magnets [21–23]. Sextupoles introduce a quadratic dependence of the particle path-length difference on energy deviation through an effective T_{566} term that, if supplied with the appropriate sign, ‘stretches’ the curvature in phase space. This mechanism is illustrated in Fig. 5. However, if the beam has to enter the undulator chain for lasing, tight tolerances on the final beam transverse emittance make the sextupole correction in a four-dipole chicane less attractive due to possible high-order magnetic aberrations. Moreover, the use of a higher-harmonic RF field does not introduce coupling between longitudinal and transverse phase-space coordinates, unlike optical manipulation of R_{56} and T_{566} terms does. For this reason, to date most of the FEL facilities have chosen to linearize the magnetic compression process with up-frequency RF structures. In principle, sextupole-induced aberrations can be counteracted with a suitable betatron phase advance between those magnets. This approach, however, implies a more sophisticated design of the chicane [24] or a different magnetic insertion [25].

It is worth noticing that a larger T_{566} term, such as the one provided by a multistage compression scheme, may be helpful in the reduction of the quadratic energy chirp induced by longitudinal geometric wake fields excited in small-iris accelerating structures [2]. The multistage compression, however, tends to amplify the so-called microbunching instability, which implies a finally increased energy spread and modulated current profile, as discussed in the next chapter.

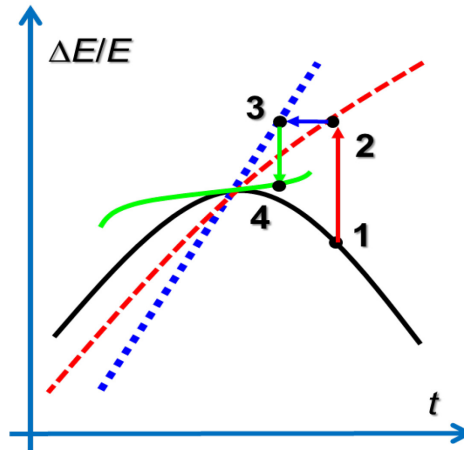


Fig. 5: Linearization of longitudinal phase space with T_{566} transport matrix element provided, e.g., by a sextupole magnet installed in a dispersive region. (1) RF curvature imprints second-order non-linearity onto the phase space (‘RF curvature’). (2) Linear energy chirp is imparted to the beam with off-crest acceleration upstream of a chicane. (3) Beam passes through a sextupole magnet in the middle of the chicane, and it is time-compressed at the chicane exit. (4) Linear chirp is removed with (opposite) off-crest phasing in a linac downstream of the chicane.

Most common geometries of magnetic insertions for bunch-length compression are shown in Fig. 6. C-shape symmetric chicanes are very common because they allow remote control of the bending angle through a translation stage of the inner dipoles, for a tuning of the compression factor and balance of momentum compaction vs. coherent synchrotron radiation (CSR) instability, which is discussed in the next chapter. The inner drift section does not contribute to the compression, but it offers room for hosting beam diagnostics and scrapers or masks for beam shaping. The chicane lateral arms may host weak quadrupole magnets for the correction of spurious dispersion function due to dipole magnet errors. Different geometries (S-shape, asymmetric tuneable C-shape and double C-shape) of the chicane have been explored in order to minimize the impact of CSR emission on the beam emittance.

In symmetric C-shape geometries, all dipoles provide the same bending angle. For any given $R_{56} \cong -2\theta_0^2 \left(L_1 + \frac{2}{3} l_d \right)$ (see Section 4 for notation), we have $T_{566} \cong -1.5 \times R_{56}$, $U_{5666} \cong 2 \times R_{56}$. For compactness, the inner dipoles can be collapsed to one magnet with double bending angle than the outer

ones. In S-shape geometries, the inner dipoles provide a bending angle larger than the outer ones. Quadrupole and sextupole magnets can interleave dipole magnets.

Arcs usually provide an R_{56} term with sign opposite to that of four-dipole chicanes, and are a natural choice for compression in recirculating machines, such as energy-recovery linacs. They may offer the chance of accommodating sextupole magnets for the linearization of the compression process, with a phase advance suitable for the cancellation of geometric and chromatic aberrations (the latter ones commonly dominate because of the relatively large relative energy spread required for compression). However, additional constraints on the linear optics functions in the bending plane are required in the arcs in order to minimize or cancel the otherwise CSR-induced projected emittance growth [26]. An arc composed of N_c fodo cells (focusing and defocusing quadrupoles alternate, interleaved by identical dipoles), with betatron phase advance μ_x per cell in the bending plane, and extending over a total length

L_{arc} , is characterized by $R_{56} \cong \frac{\theta_0^2 L_{arc}}{4N_c^2 \sin^2(\mu_x/2)}$; with no sextupoles included, $T_{566} \approx 2 \times R_{56}$ or larger. A

dog-leg can be built with two consecutive arc-fodos. For the simplest two-dipole symmetric geometry, the dog-leg features $R_{56} \cong \theta_0^2 l_d / 3$. A series of double- or multibend achromatic cells can be used to build up an arc of arbitrary bending angle. In a periodic arc made of N_c identical symmetric double-bend achromatic cells, $R_{56} \cong 2N_c \theta_0^2 l_d$.

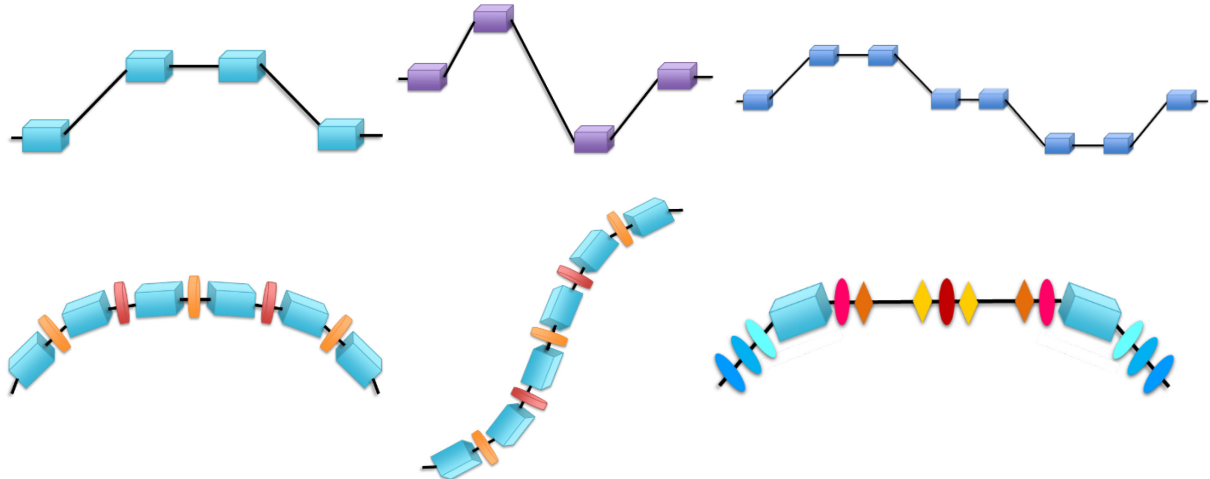


Fig. 6: Most common geometries (not to scale) of magnetic insertions for bunch-length compression. From top, left to right: C-shape, S-shape and double C-shape chicanes; bottom, arc-fodo, dog-leg-fodo and double-bend achromatic cells.

7 Jitter of bunch arrival time and compression factor

FELs usually require tight control of the electron-beam arrival time at the undulator. The shot-to-shot reproducibility of the arrival time of consecutive electron bunches, henceforth named ‘arrival time jitter’ (ATJ), is of great importance for multishot experiments. On the single-pulse basis, it is even more important for FELs driven by an external laser (externally seeded FELs), in order to ensure synchronism between the laser and the electron bunch. The requirement of small ATJ is particularly stringent when the electron bunch is longitudinally compressed to sub-ps durations, in order for the jitter to be (much) smaller than the bunch duration. Following Ref. [27], we introduce a model for the ATJ in the presence of magnetic compression in a four-dipole chicane, like the one sketched in Fig. 2. The error sources contributing to the ATJ we consider are: photo-injector laser arrival time on the cathode, jitter of phases and voltages of the RF linac and fluctuations of the compressor’s dipole field, as may be produced by fluctuations of the power converters.

We adopt the bunch centroid as the reference particle. Its final time coordinate in the laboratory frame is $t_f = t_i + \frac{\Delta l + L}{c}$, where t_i is the reference initial arrival time, L is the straight trajectory length through the chicane (zero bending angle) and Δl is the path-length difference between the beam trajectory through the chicane with dipoles turned on and the straight trajectory. If $\theta \ll 1$, one finds [13] $\Delta l \cong -R_{56}/2$. The ATJ after the beam has passed through an RF linac and one chicane is

$$\begin{aligned} cdt_f &= cdt_i + d(\Delta l) = cdt_i + \frac{\partial(\Delta l)}{\partial E} dE + \frac{\partial(\Delta l)}{\partial B} dB \\ &= cdt_i + \frac{\partial(\Delta l)}{\partial \theta} \frac{\partial \theta}{\partial E} dE + \frac{\partial(\Delta l)}{\partial R_{56}} \frac{\partial R_{56}}{\partial \theta} \frac{\partial \theta}{\partial B} dB \cong cdt_i + \frac{R_{56}}{E} dE - \frac{R_{56}}{B} dB, \end{aligned} \quad (17)$$

where E is the beam mean energy at the chicane and B is the dipoles' magnetic field. The last equality makes use of the expressions for the dipole length $l_d = R \sin \theta$ and of the curvature radius $R = E/(eBc)$. The differential of the beam energy w.r.t. the variation of the peak voltage, RF phase and arrival time at the linac entrance, is $dE = e \cos \phi dV - eV \sin \phi d\phi - eV k_{rf} \sin \phi dt_i$. Substituting it into Eq. (17), and also introducing the linear compression factor C (see Eq. (12)), we obtain

$$\begin{aligned} dt_f &\cong dt_i + \frac{R_{56}}{c} \left(\frac{\cos \phi}{E} edV - \frac{eV \sin \phi}{E} d\phi - \frac{eV k_{rf} \sin \phi}{E} dt_i - \frac{dB}{B} \right) \\ &= \frac{dt_i}{C} + \frac{R_{56}}{c} \left(\frac{\cos \phi}{E} edV - \frac{eV \sin \phi}{E} d\phi - \frac{dB}{B} \right). \end{aligned} \quad (18)$$

We now move from the single-particle picture in Eq. (18) to the rms value of the ATJ, where all the jitter sources are assumed to be small and independent perturbations to the particles' motion:

$$\sigma_{t,f}^2 \cong \left(\frac{\sigma_{t,i}}{C} \right)^2 + \left(\frac{R_{56}}{c} \right)^2 \left[\left(\frac{eV \cos \phi}{E} \right)^2 \left(\frac{\sigma_V}{V} \right)^2 + \left(\frac{eV \sin \phi}{E} \right)^2 \sigma_\phi^2 + \left(\frac{\sigma_B}{B} \right)^2 \right]. \quad (19)$$

If no additional dispersive insertions are foreseen between the chicane and the undulator, the ATJ at the exit of the chicane will be frozen up to the end of the beam line. Reduction of the ATJ at the entrance of the chicane by the compression factor is due to the fact that an earlier (later) arrival of the bunch centroid to the RF field in the upstream linac translates, e.g., to a lower (higher) energy at the chicane, and therefore to a shorter (longer) path length with respect to the reference trajectory.

The linac peak voltage jitter maximally (minimally) contributes to the ATJ for the linac operated on crest (at zero crossing). For on-crest operation, the RF phase jitter term can usually be neglected as long as the bunch length is much shorter than the RF wavelength. This opposite behaviour of the two RF jitter sources as a function of the RF phase, suggests the possibility of choosing the RF linac phase in a way that, for any specified error budget, the ATJ is minimum [27]. Although quite an attractive option in principle, such an optimal linac configuration constrains the compression factor to some specific values or to a limited range, for any given setting of the magnetic chicane. In the case of multistage compression schemes, more RF settings are available that may simultaneously ensure the lowest ATJ for a design compression factor, energy spread and chicane bending angle.

A jitter of the compression factor implies a jitter of the final bunch length or of the final peak current, for initially constant bunch length and bunch charge. Owing to the fact that the linac upstream

of the chicane is run off-crest in practical cases, the jitter of C is dominated by the RF phase jitter. We therefore differentiate the expression for C assuming that only the RF phase varies (namely, we neglect any variation of linac peak voltage and dipole field):

$$\begin{aligned}\Delta\left(\frac{1}{C}\right) &= -\frac{\Delta C}{C^2} = \Delta(1 + hR_{56}) \cong R_{56} \frac{\Delta h}{h} h \cong R_{56} \frac{\Delta(\sin\phi)}{\sin\phi} h = hR_{56} \frac{\Delta\phi}{\tan\phi}, \\ \frac{\Delta C}{C} &\cong -ChR_{56} \frac{\Delta\phi}{\tan\phi} = (C-1) \frac{\Delta\phi}{\tan\phi}, \\ \sigma_C^2 &\cong (C-1)^2 \frac{\sigma_\phi^2}{\tan^2\phi}.\end{aligned}\tag{20}$$

Equation (20) shows that the *relative* jitter of C is proportional to C itself and that, for any given RF phase jitter, it is maximum for the phase set at zero crossing.

8 RF compression

RF compression [28] refers to two techniques of bunch-length shortening that exploit the relative longitudinal slippage of low-energy electrons as induced by a suitable arrangement of the RF linac phase. In RF ‘ballistic bunching’, an energy chirp is imparted to the beam in a cavity run off-crest. If the beam energy is low enough (particles are *not* in the *ultra*-relativistic limit yet), a difference in longitudinal momentum translates into a difference in longitudinal velocities, and therefore in arrival time at a given position downstream of the cavity. In order for a ~ 10 MeV bunch to be shortened by, say, a factor ~ 5 , a drift length of the order of ~ 1 m or longer may be needed after the cavity. Bunch shortening happens if the bunch head is at lower energies than the bunch tail. Most of bunch shortening happens outside the cavity, and the energy–position correlation established in the cavity tends to be removed later in the drift section. However, the final longitudinal phase space usually shows strong nonlinearities as induced by both the RF curvature and space-charge forces, which are enhanced by the increased charge density [29].

RF ‘velocity bunching’ differs from ballistic bunching in that the phase-space rotation happens *inside* an RF linac, still run off-crest, and the energy chirp is smoothly removed in the linac itself through electrons’ longitudinal slippage and acceleration. Similarly to the ballistic bunching, the minimum bunch length achievable with this technique is determined by the distortion of the final phase space induced by RF field nonlinearities and space-charge forces.

In order to follow the longitudinal particle motion in the presence of RF compression, we assume the beam to be accelerated in a (series of) SW structure(s), which were introduced in Section 3. The evolution of the beam mean energy gain and the beam arrival time along the beam line is

$$\begin{aligned}\frac{d\gamma(s)}{ds} &= \alpha [\cos(\phi) + \cos(\phi + 2ks)], \\ dt = \frac{ds}{\beta c} &= ds \frac{\gamma(s)}{c\sqrt{\gamma(s)^2 - 1}},\end{aligned}\tag{21}$$

where we introduced the ‘electron capture’ parameter $\alpha \equiv \frac{eE_{z,0}}{2km_e c^2}$ and the RF phase ϕ ; the factor ‘2’ in α disappears for TW structures. The physical meaning of such a normalized strength of the accelerating

field is that, for values larger than 1, the particle dynamics shows relativistic effects within one period of the RF wave.

Following Ref. [30], we notice that dt (equivalent to beam phase) changes considerably near the cathode, where the electrons are still not or weakly relativistic. In that region s is small and we integrate Eq. (21) as follows:

$$\begin{aligned}\gamma(s \approx 0) &\approx 1 + 2k\alpha s \cos \phi, \\ \phi(s) &= \phi_0 + \int_0^s d(\omega t - ks + \varphi) \approx \phi_0 + k \int_0^s dt \frac{\gamma(s)}{\sqrt{\gamma(s)^2 - 1}}.\end{aligned}\quad (22)$$

We now insert the upper expression of Eq. (22) in the lower one, to find an approximate expression for the beam phase. The latter will be inserted into Eq. (21) again to find a more accurate expression for the energy gain. Eventually, we find

$$\begin{aligned}\gamma(s) &\cong 1 + \alpha \left\{ ks \cos \phi(s) - \frac{1}{2} [\sin(\phi) - \sin(\phi + 2ks)] \right\}, \\ \phi(s) &\cong \phi_0 - \frac{1}{2\alpha \cos \phi_0} \left[\sqrt{\gamma^2 - 1} - (\gamma - 1) \right]_{(s \approx 0)} \rightarrow \phi_\infty = \phi_0 - \frac{1}{2\alpha \cos \phi_0}.\end{aligned}\quad (23)$$

The asymptotic value of the beam phase in Eq. (23) is for $\gamma \gg 1$. Figure 7 shows particle trajectories in the longitudinal phase space as depicted by Eq. (23). In that example, acceleration is maximum for $\varphi = \pi/2$.

A rough estimation of the bunch length compression factor in the limit of high beam energy can be obtained by recalling that bunch-length shortening means also compression of an incoming time or phase jitter (see Section 7). We differentiate the phase expression in Eq. (23) and find

$$C \approx \frac{d\phi_0}{d\phi_\infty} = \left[1 - \frac{\sin \phi_0}{2\alpha \cos^2 \phi_0} \right]^{-1}.\quad (24)$$

For example, for $\alpha = 2$ and $\varphi_0 = \pi/3$, $C \approx 10$.

Although neglected so far, the longitudinal particle dynamics at beam energies as low as considered in this section is intrinsically coupled to the transverse one by means of the repulsive 3D space-charge forces. In practical situations, the compression factor achieved through RF compression is limited by the tolerable transverse emittance dilution induced by space-charge forces. This effect can be mitigated by the application of external magnetic focusing, such as solenoidal fields, that counteract the particles' repulsion ('emittance compensation') [31].

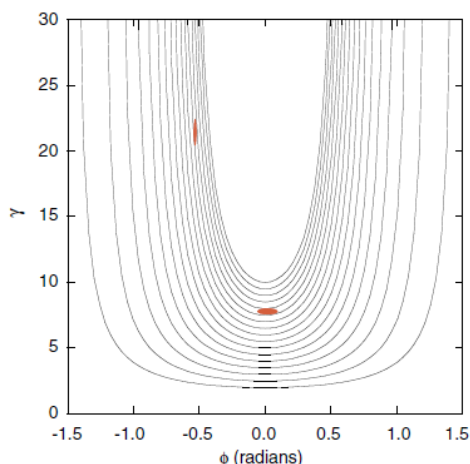


Fig. 7: Phase-space apparent rotation in RF sinusoidal accelerating field, leading to bunch-length shortening for a bunch injected near the phase of zero crossing. Published in Ref. [29]. Copyright of American Physical Society.

Acknowledgement

The author wishes to thank M. Venturini for his invaluable guidance through the physics of bunch-length compressors, and for his contribution to Figs. 2 and 3 of this chapter. P. Craievich and M. Cornacchia are acknowledged for careful reading of this work and for suggestions.

References

- [1] K. Cohn *et al.*, Proc. 37th Free Electron Laser Conf., WEP016, Daejeon, Korea, 2015.
- [2] S. Di Mitri and M. Cornacchia, *Phys. Rep.* **539** (2014) 1.
<https://doi.org/10.1016/j.physrep.2014.01.005>
- [3] C. Lejeune and J. Aubert, in *Applied Charged Particle Optics*, Ed. A.L. Septier (Academic Press, New York, 1980), pp. 159–259.
- [4] R. Bonifacio, C. Pellegrini and L.M. Narducci, *Opt. Commun.* **50** (1984) 373.
[https://doi.org/10.1016/0030-4018\(84\)90105-6](https://doi.org/10.1016/0030-4018(84)90105-6)
- [5] W.B. Colson, *IEEE J. Quant. Electron.* **17** (1981) 1417.
<https://doi.org/10.1109/JQE.1981.1071273>
- [6] C. Pellegrini, *Eur. Phys. J. H* **37** (2012) 659. <https://doi.org/10.1140/epjh/e2012-20064-5>
- [7] A.M. Kondratenko and E.L. Saldin, *Part. Accel.* **10** (1980) 207.
- [8] P. Sprangle, C.-M. Tang and W.M. Manheimer, *Phys. Rev. A* **21** (1980) 302.
<https://doi.org/10.1103/PhysRevA.21.302>
- [9] K.-J. Kim, *Nucl. Instrum. Methods Phys. Res. A* **246** (1986) 71. [https://doi.org/10.1016/0168-9002\(86\)90048-3](https://doi.org/10.1016/0168-9002(86)90048-3)
- [10] S. Di Mitri, *Photonics* **2** (2015) 317. <https://doi.org/10.3390/photonics2020317>
- [11] P.M. Lapostolle and A.L. Septier, Eds., *Linear Accelerators* (North-Holland, Amsterdam, The Netherlands, 1970), pp. 30–47.
- [12] K.L. Brown, *Adv. Part. Phys.* **1** (1968) 71 and SLAC-75 Rev. 4 (1982).
- [13] P. Castro, DESY Technical Note TN-2003-01 (2003).
- [14] P. Emma, LCLS Report LCLS-TN-01-1 (2001).
- [15] K.L.F. Bane and P. Emma, Proc. 2005 Particle Accelerator Conf., Knoxville, TN, USA, 2005, pp. 4266–4268. <https://doi.org/10.1109/PAC.2005.1591786>

- [16] K. Flöttmann, T. Liberg and Ph. Piot, DESY Technical Note TESLA-FEL-2001-06 (2001).
- [17] K.L.F. Bane, *Int. J. Mod. Phys. A* **22** (2007) 3736. <https://doi.org/10.1142/S0217751X07037391>
- [18] I. Zadorodnov and M. Dohlus, *Phys. Rev. ST Accel. Beams* **14** (2011) 014403.
<https://doi.org/10.1103/PhysRevSTAB.14.014403>
- [19] M. Cornacchia *et al.*, *Phys. Rev. ST Accel. Beams* **9** (2006) 120701.
<https://doi.org/10.1103/PhysRevSTAB.9.120701>
- [20] P. Craievich, *Phys. Rev. ST Accel. Beams* **13** (2010) 034401.
<https://doi.org/10.1103/PhysRevSTAB.13.034401>
- [21] P. Piot, D.R. Douglas and G.A. Krafft, *Phys. Rev. ST Accel. Beams* **6** (2003) 030702.
<https://doi.org/10.1103/PhysRevSTAB.6.030702>
- [22] R.J. England *et al.*, *Phys. Rev. ST Accel. Beams* **8** (2005) 012801.
<https://doi.org/10.1103/PhysRevSTAB.8.012801>
- [23] P. Evtushenko, S. Benson and D. Douglas, Proc. 10th European Workshop on Beam Diagnostics and Instrumentation, MOOB04, Hamburg, Germany, 2011.
- [24] Y. Sun, *et al.*, *Phys. Rev. ST Accel. Beams* **17** (2014) 110703.
<https://doi.org/10.1103/PhysRevSTAB.17.110703>
- [25] S. Thorin *et al.*, Proc. 32nd Int. Free Electron Laser Conf., WEPB34, Malmö, Sweden, 2010.
- [26] S. Di Mitri and M. Cornacchia, *Eur. Phys. Lett.* **109** (2015) 62002.
<https://doi.org/10.1209/0295-5075/109/62002>
- [27] P. Craievich *et al.*, *Phys. Rev. ST Accel. Beams* **16** (2013) 090401.
<https://doi.org/10.1103/PhysRevSTAB.16.090401>
- [28] L. Serafini and M. Ferrario, *Physics of, and Science with, the X-Ray Free-Electron Laser*, Eds. S. Chattopadhyay, M. Cornacchia, I. Lindau and C. Pellegrini (AIP Conf. Proc. 581) (AIP, New York, 2001).
- [29] S.G. Anderson *et al.*, *Phys. Rev. ST Accel. Beams* **8** (2005) 014401.
<https://doi.org/10.1103/PhysRevSTAB.8.014401>
- [30] K.-J. Kim, *Nucl. Instrum. Methods Phys. Res. A* **275** (1989) 201. [https://doi.org/10.1016/0168-9002\(89\)90688-8](https://doi.org/10.1016/0168-9002(89)90688-8)
- [31] M. Ferrario *et al.*, *Phys. Rev. Lett.* **104** (2010) 054801.
<https://doi.org/10.1103/PhysRevLett.104.054801>

Bibliography

Proceedings of the CAS-CERN Accelerator School: Fifth General Accelerator Physics Course, 7 - 18 Sep 1992, Jyväskylä, Finland, edited by S. Turner, CERN-1994-001 (CERN, Geneva 1994). <https://doi.org/10.5170/CERN-1994-001>.

I.S. Ko and W. Chou, Eds., ICFA Beam Dynamics Newsletter No. 38 (2005).

P. Schmuser, M. Dohlus and J. Rossbach, in *Ultraviolet and Soft X-ray Free-Electron Lasers*, Eds. A.F. Chiba *et al.* (Springer Tracts Mod. Phys. 229) (Springer, Berlin, 2008).